



Preparation of a novel hafnium-loaded $\text{Fe}_3\text{O}_4@\text{SiO}_2$ superparamagnetic nanoparticles and its adsorption performance for phosphate in water

Gege Zhao^{a,b}, Qian Zhao^{a,b,c,*}, Xinwei Jin^{c,a}, Hongbo Wang^{a,b}, Kefeng Zhang^{a,b}, Mei Li^{a,b,*}, Ning Wang^{a,b}, Wenxiu Zhao^d, Shujuan Meng^e, Ruimin Mu^{a,b}

^aSchool of Municipal and Environmental Engineering, Shandong Jianzhu University, 1000 Fengming Road, Jinan 250101, China, Tel. +86-531-86361857; emails: zhaoqian@sdjzu.edu.cn (Q. Zhao), gege19951101@163.com (G. Zhao), wanghongbo@sdjzu.edu.cn (H. Wang), kfzhang@sdjzu.edu.cn (K. Zhang), limei@sdjzu.edu.cn (M. Li), wangning@sdjzu.edu.cn (N. Wang), xiaomu@sdjzu.edu.cn (R. Mu)

^bShandong Province Co-Innovation Center of Green Building, Jinan 250101, China

^cGuangdong Provincial Key Laboratory of Environmental Pollution Control and Remediation Technology, Sun Yat-sen University, Guangzhou 510275, China

^dSIIC Environment Holding Co., Ltd., Weifang 261061, China, email: 13563696627@163.com

^eSchool of Space and Environment, Beihang University, Beijing 100191, China

Received 26 March 2020; Accepted 26 October 2020

ABSTRACT

Phosphorus is an essential element of life but can lead to eutrophication if present above limit in waterways. Hydrous metallic oxides-based magnetic nanoparticle is considered as an easily separable adsorbent for efficient separation of phosphate from sewage. In this paper, superparamagnetic particles consisting of hafnium-modified hydroxides loading on Fe_3O_4 multicores embedded in SiO_2 matrix were synthesized (MgFeHf-NPs/MgAlHf-NPs) and the performance of capturing phosphate was investigated. The obtained nano-composites showed well-defined crystal structure and sufficient saturation magnetization. High phosphate adsorption capacity was observed with these NPs from solution as well as digested sludge liquor and dewatered sludge wastewater. These NPs also showed high selectivity with other co-existing ions and organics. The enhancement of phosphate adsorption capacity by doping with Hf should be explained by the stronger ligand complexation built by the pair of the hard acid Hf ion and the hard base phosphate that matched up the bonding preferences. MgAlHf-NPs and MgFeHf-NPs exhibited regeneration rates after five adsorption-desorption cycles compared with ordinary MgAl-NPs and MgFe-NPs. This paper attempts to provide a promising nano-sorbent for phosphate recovery.

Keywords: Phosphate recovery; Phosphate absorption; Nanoparticles; Superparamagnetic; Reusability

1. Introduction

Phosphorus plays an important role in the process of biological growth and human development, and it is also a non-renewable resource. With the development and utilization of global phosphate mineral resources, its storage and

consumption rate has accelerated. High-grade phosphate rock reserves will be depleted in the coming decade [1]. Thus, recovering phosphorus from sewage wastewater is imperative and a feasible option against phosphorus crisis.

At present, struvite and hydroxyl calcium phosphate crystallization method is a widely used P-recovery

* Corresponding authors.

methods in practice [2,3]. However, the production of struvite requires harsh crystallization conditions and the pretreatment of qualified fertilizers is more complicated, which vastly obstructs its application [4,5]. The crystallization method also requires the alkaline nature of the incoming water, therefore, increase the cost of dosing additional chemicals [6]. Moreover, the organic compounds in the sewage have an interferential effect on the crystallization performance [7]. The produced chemical sludge also faces the disposal problem. The biological phosphorus removal methods including artificial wetland [8], anaerobic/aerobic (A²/O) process [9,10] and enhanced biological phosphorus removal process [11], etc. can efficiently transfer the phosphorus from wastewater to the excess sludge. In recent years, the researchers have developed a variety of P-capture adsorbents, among which superparamagnetic nanoparticles seemed promising due to their large phosphate uptake capacity, high selectivity in presence of coexisting foreign species, fast separation, and recyclability [12]. These superparamagnetic nanocomposite material effectively turns “removal of phosphorus” into “recovery of phosphorus”, which fundamentally solves the problems of phosphorus pollution and shortage of phosphorus resources in water bodies.

Superparamagnetic nanocomposites are complexed matrix containing Fe₃O₄ core with high magnetization and hydroxide species, hydroxides or layered double hydroxides (LDHs) on the surface, which serve as the center for phosphate adsorption [13]. The used composite can be washed and regenerated in caustic soda (NaOH) or KOH solution. Moreover, the magnetic P adsorbents exhibited improved adsorption capacity after doping with oxides of transition metals or rare earth metals, such as lanthanum, zirconium, etc. [14]. For example, Drenkova-Tuhtan et al. [12] tested the superparamagnetic nanocomposite particles functionalized by Zn-Fe Zr adsorbent. Under the optimal conditions, the total phosphorus recovery efficiency can be more than 90%.

Lai et al. [15] loaded a trace amount of hydrated lanthanum oxide on Fe₃O₄@SiO₂ (Fe-Si-La) to acquire adsorbent capability of magnetic separation. The established Fe-Si-La matrix improved the Langmuir adsorption capacity of phosphate [15]. Zhang et al. [16] prepared magnetic nanoparticles with different Fe/Zr molar ratios. The effect of these adsorbents is highly pH dependent: the adsorption capacity decreases gradually in the pH range of 1.5–10 [16]. It seemed that doping with these metals might change not only the adsorption capacity and the reusability but also the adsorption behavior during adsorption–desorption cycles.

Hf is a strong paramagnetic metal without negative environmental impacts. Besides, it is both hard Lewis acid and 5d-transitional metal of large size, therefore presumably forming strong ligand complexation with phosphate. None of the previous studies have tried Hf-doped nano-sorbent to sequester phosphate from sewage. The research contents of the paper included (1) preparation and characterization of superparamagnetic nano-adsorbents by loading hafnium oxide on the surface of MgAl-NPs/MgFe-NPs Fe₃O₄@SiO₂ NPs (denoted as MgAlHf-NPs/MgFeHf-NPs); (2) exploration of the phosphorus removal effect of NPs, including the adsorption efficiency, adsorption isotherm,

and the effects of coexisting anions and biomacromolecules; (3) detection of desorption degree and regeneration efficiency of new magnetic separation adsorbent; (4) discuss the enhancement mechanism of the doped metals on the phosphate adsorption within the superparamagnetic nano-sorbent matrix; (5) compare the hafnium-modified NPs developed in this study and other superparamagnetic nano-sorbents reported previously.

2. Materials and methods

2.1. Synthesis of Hf-coated superparamagnetic NPs

2.1.1. Synthesis of Fe₃O₄@SiO₂ superparamagnetic NPs

Preparation of Fe₃O₄@SiO₂ superparamagnetic micro-particles requires two steps: synthesis of magnetite and coating with silica. Synthesis of magnetite was conducted according to co-precipitation method. Specifically, 8.64 g FeCl₃·6H₂O (Sinopharm Chemical Reagent Co. Ltd., Shanghai) and 3.18 g FeSO₄·7H₂O (Sinopharm Chemical Reagent Co. Ltd., Shanghai) (2:1 in molar ratio) were dissolved in 100 mL deionized water, which had been deoxygenated with a desiccator connecting to a vacuum pump for 30 min. Meanwhile ammonium hydroxide (Fuyu Fine Chemicals Co. Ltd., Tianjin) of 1.5 mol/L was added into the solution dropwise with stirring at room temperature. When the final pH value reaches 8, stirring was stopped, the black mixture was separated with magnetic force, it was washed with deionized water for three times, and it was dried in the freeze dryer. All the chemicals employed in the preparation step were all AR grade.

The suspension was mixed with 120 mL nitric acid (0.66 M; Huiyuan Fine Chemicals Co. Ltd., Laiyang). The solution was further stabilised by carboxylic acid. The resulting solution had a pH of 1–2. Ammonium hydroxide (88 mL of 25 wt.%) diluted in 80 mL deionized water was added to the functionalised nanoparticle solution. After heating the blend to 70°C, sodium silicate was added (Damao Chemical Reagent Co. Ltd., Tianjin) solution drop by drop with syringe under stirring mole ratio: NH₄OH:HNO₃:Na₂SiO₃ = 27:1:0.4. After agitating for 5 min, the silicified magnetite was magnetically settled and washed three times with deionized water.

2.1.2. Synthesis of Hf-loaded hydroxides

A certain amount of a combination of different metal salts such as MgCl₂·6H₂O (Sinopharm Chemical Reagent Co. Ltd., Shanghai), AlCl₃·6H₂O (Sinopharm Chemical Reagent Co. Ltd., Shanghai), HfOCl₂·8H₂O (Alfa Aesar Chemical Co. Ltd.) were dissolved in 100 mL deionized water to prepare precursor solutions of different hydroxides (40 wt.%; Table 1). The precursor solution was gradually put into 400 mL of a 0.15 M NaOH solution for 5 min with uniform stirring and then adjusted the pH to 7 with HCl (Huiyuan Fine Chemicals Co. Ltd., Laiyang).

2.1.3. Loading hydroxides onto Fe₃O₄@SiO₂ NPs

Different hydroxide liquid were mixed with silica coated magnetite dispersed suspensions prepared in section 2.1.1

Table 1
Preparation of metal ion precursor solution

Sample	MgCl ₂ ·6H ₂ O	AlCl ₃ ·6H ₂ O	FeCl ₃ ·6H ₂ O	HfOCl ₂ ·8H ₂ O
MgAl	16 mmol	8 mmol	–	–
MgFe	17.4 mmol	–	5.8 mmol	–
MgAlHf	16 mmol	8 mmol	–	8 mmol
MgFeHf	17.4 mmol	–	5.8 mmol	5.8 mmol

for 60 s under stirring. The dispersions were subsequently placed into an ultrasonic bath (Kunshan Ultrasonic Instruments Co., Ltd.: KQ3200 V, 180 W, 35 kHz) for 100 s. Then, the solid phase, that is, the superparamagnetic NPs, was magnetically separated and washed with deionized water (twice) then lyophilized by a freeze dryer, and the powder is stored for subsequent characterization and adsorption/desorption test. The magnets employed were NdFeB permanent ring (Ø24*5) magnets with NiZn coating having a magnetic flux density of 1.26 T (Shanghai Shengci Magnetic Instrument Co. Ltd.).

2.2. Characterization of materials

The surface configuration of the materials was analyzed with scanning electron microscope (SEM, ZEISS Gemini SUPRA55, Oberkochen, Germany) with the energy dispersive spectrometer and transmission electron microscope (TEM, JEM-2100). Prior to the observation, the samples were first pretreated by coating after dispersing them into ethal with sonication. The chemical composition was analyzed by X-ray fluorescence (XRF, Thermo Scientific Niton XL5, Waltham, USA) and the X-ray diffraction analysis was also carried out (XRD, Smartlab). The NPs' saturated magnetization was measured through plotting magnetization vs. magnetic field (M-H) curves with a vibrating sample magnetometer (Micro Sence EZ7).

2.3. Adsorption experiments

A certain amount of KH₂PO₄ (Sinopharm Chemical Reagent Co. Ltd., Shanghai) was dried in an electric blast drying oven (GZX-9140MBE) at 110°C for 3 h and then taken out. After KH₂PO₄ was added into a desiccator and cooled to room temperature, 2.1985 g was weighed and dissolved in water, and the volume was fixed to a 1,000 mL volumetric flask to obtain a phosphate stock solution of 500 mg P/L. Other concentrations of phosphate solutions required in the experiment can be obtained from the stock solution. A batch adsorption test kinetic was conducted by exposing 0.05 g of dry mass of MgAl-/MgFe-/MgAlHf-/MgFeHf-NPs, respectively, to a 100 mL aqueous solution (corresponding NPs dosage: 500 mg P/L) containing phosphate with concentrations ranging from 5 to 80 mg P/L. pH was adjusted at optimal value of 4.5 with 1 mol/L consistency of HCl or NaOH. The optimal pH value was pre-determined in a pH-dependent experiment (Fig. 1). The flasks were capped and shaken vigorously in a shaker at 120 rpm for 1 h to reach adsorption equilibrium, which was

pre-determined via an adsorption equilibrium test at room temperature (Fig. 2). Then the supernatant was decanted through a magnet and the phosphate concentration was determined by using the molybdenum blue method with UV-1780 spectrophotometer (Shimadzu, Kyoto, Japan) [17]. Thus, q_e (mg/g), the amount of phosphate loaded per unit mass of adsorbent at the equilibrium, that is, the maximal adsorption capacity can be determined. The phosphorus abscission efficiency (%) also can be calculated.

The adsorption capacity for phosphate at diverse equilibrium concentrations could be described by adsorption isotherms. To fit the balance information, Langmuir and Freundlich isotherm models were used, with equations defined as below:

$$q_e = \frac{q_m K_L C_e}{(1 + K_L C_e)} \quad (1)$$

$$q_e = k_f C_e^{1/n} \quad (2)$$

where C_e (mg/L) is the phosphate equilibrium concentration in aqueous phase. K_L (L/mg) and k_f ((mg/g)/(mg/L)^{1/n}) are, respectively, the Langmuir and Freundlich adsorption equilibrium constants. n is a constant indicating the Freundlich isotherm curvature.

2.4. Effect of coexisting substances on phosphate adsorption

In the study on the competing effect of coexisting substances, phosphate with initial concentration of 5 mg/L was mixed with 10 mM Cl⁻ (NaCl, Sinopharm Chemical Reagent Co. Ltd., Shanghai), 10 mM SO₄²⁻ (Na₂SO₄, Sinopharm Chemical Reagent Co. Ltd., Shanghai), 10 mM CH₃COONa (Sinopharm Chemical Reagent Co. Ltd., Shanghai), polysaccharide (100 mg/L sodium alginate, Merck, Darmstadt, Germany) and protein (100 mg/L bovine serum albumin, Merck, Darmstadt, Germany) solutions separately. 0.1 g MgAl-, MgFe-, MgAlHf-, MgFeHf-NPs were dosed into 100 mL of each mixture above. The solution pH was all controlled at about 4.5 with nitric acid (no competing effect confirmed by pre-test), and the contact time was 1 h. Then phosphate removal efficiency (%) with coexisting substances was calculated.

2.5. Adsorption for digested sludge liquor (DSL) and dewatered sludge wastewater (DSW)

The Hf-loaded NPs were employed to treat the DSL and DSW, which was obtained from thermophilic digesters

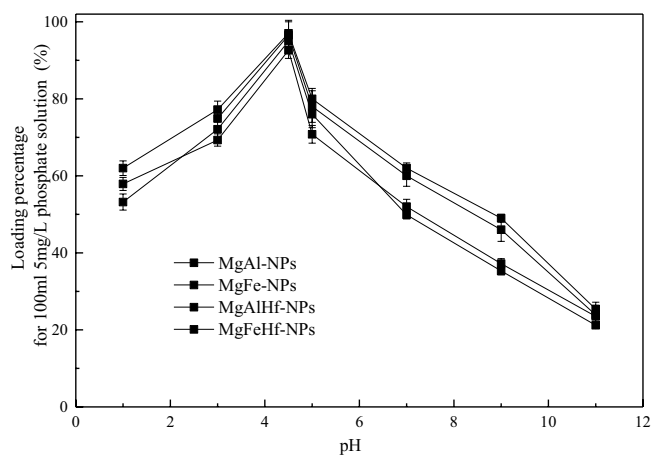


Fig. 1. Adsorption of phosphate on NPs as a function of pH variation.

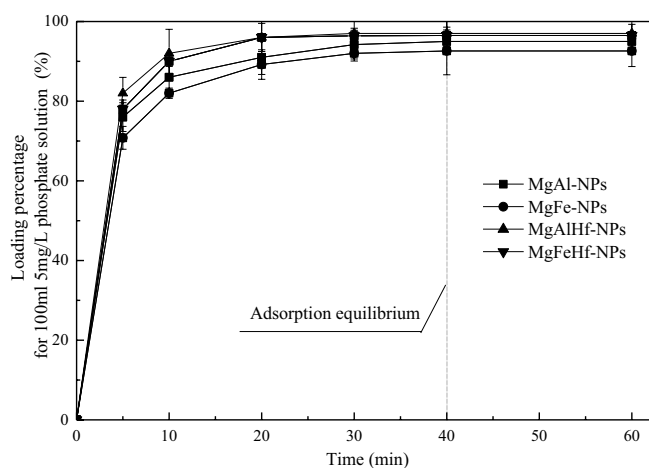


Fig. 2. Adsorption equilibrium of phosphate adsorption on NPs.

and full-scale WWTP. The relevant information about the reactors and water quality has been presented in our previous study (Table 4). DSL was obtained from the lab-scale thermophilic digesters (operating at 55°C), which were fed with excess sludge from A²O tank in a WWTP (Plant 1) in Liaocheng and a lab-scale EBPR reactor synthetic treating domestic wastewater (Plant 2) was, respectively, added. DSW was the filtrate from dewatering the DSL in plants 1 and 2 with vacuum filter. 100 mL DSL, DSW in plant 1 was blended with 0.3 g MgFeHf-NPs, acidified DSL/DSW plant 1 and DSL/DSW in plant 2 was mixed with 0.8 g MgFeHf-NPs, and acidified DSL/DSW plant 2 was mixed with 1.5 g MgFeHf-NPs. The organic phosphorus (or-P) and total dissolved phosphate (t-P) in decanted supernatant were measured for each pH value by standard method. Or-P in wastewater samples was determined by subtracting dissolved acid hydrolysable phosphorus and dissolved reactive phosphorus from total dissolved acid-digested phosphorus. The protein and polysaccharide of extracellular polymeric substances were determined by the Lowry method [18] and anthrone colorimetry [19], respectively. The specimen was leached through a 0.45 μm filter before analysis and

adsorption test. The pH was measured using a pH electrode (Leici PHS-25). The consistence of Fe³⁺, Ca²⁺, Mg²⁺, Al³⁺ and Zn²⁺ were then quantified using inductively coupled plasma atomic emission spectrophotometer (ICP-AES, iCap 6300 DUO; Thermo Scientific, Waltham, MA, USA). All the analyses were performed in triplicates.

2.6. Desorption and regeneration experiments

The desorption experiment was conducted with four types of phosphate-loaded nanoparticles, that is, 0.05 g MgAl-/MgFe-/MgAlHf-/MgFeHf-NPs, which have been contact with 5 mg P/L in adsorption test. After the adsorption reached equilibrium, these sorbents were separated with a magnet and washed with deionized water, desorption of adsorbed phosphate from the sorbent was done by adding 100 mL 2 M NaOH solution at 30°C. After 24 h contact and then a solid/liquid separation with a magnet again, the phosphate amount in the supernatant, marked as Q_i (mg) can be determined using the molybdenum blue method and recovery rate P_i can be calculated. Then the re-adsorption and re-desorption tests were repeated four times with retrieved nano-sorbents above by dosing them in 100 mL 5 mg P/L phosphate solution and regenerating them with NaOH solution again, repeating the procedures above. For the i th cycle of adsorption and desorption test, phosphate recovered amount Q_i and recovery rate P_i were calculated using the equation below:

$$P_i = \frac{Q_i}{(5 \text{ mg/L} \times 0.1 \text{ L})} \quad i = 1, 2, 3, \dots, 10 \quad (3)$$

Finally, the recovery rate P_i for all the materials for each cycle was plotted in the form of heatmap. All the presented data are mean value of triplicate experiments.

3. Results and discussion

3.1. Structural characterizations of the microparticles

The chemical constitution of materials is listed in Table 2. The proportion (wt.%) of Mg, Al, Fe, Si and Hf in MgAlHf- and MgFeHf-NPs as well as the trivial impurities (<1%) implied the magnetites, hydroxides, including the hydrous hafnium oxides were successfully incorporated in the nano-sorbent. According to the data in Table 2, the mole ratio of Mg:Al:Hf was about 0.11:0.065:0.072, which was very close to the molar ratio of 2:1:1 in the precursor solutions employed in the synthesis step in section 2.1.2. Larger proportion of Fe in MgFe- and MgFeHf-NPs could be explained by the ferrous components in both hydroxides and magnetite cores.

Surface structure of bare Fe₃O₄@SiO₂, MgAl- and MgAlHf-NPs can be observed in the representative SEM and TEM micrographs in Fig. 3. The SEM and TEM pattern of NPs are presented in Figs. 3a–g, respectively. All the types of composites had relatively regular shapes and smooth surfaces, without any noticeable difference among them except for seemingly rough surface for the Hf-coated ones. For both bare Fe₃O₄@SiO₂ and nano-sorbent,

Table 2
Compositions and proportions of chemical elements in NPs revealed by XRF

Samples	Al (%)	Mg (%)	Fe (%)	Hf (%)	Na (%)	Si (%)	O (%)	Cl (%)	Other (%)
MgAl-NPs	2.06	3.37	25.50	0	2.55	1.91	62.94	1.47	0.20
MgAlHf-NPs	1.75	2.65	26.29	12.94	1.13	0.84	52.48	1.72	0.21
MgFe-NPs	0.21	3.60	32.03	0	1.55	1.81	58.62	1.91	0.27
MgFeHf-NPs	0.13	2.44	25.89	8.28	5.94	0.82	51.18	5.15	0.18

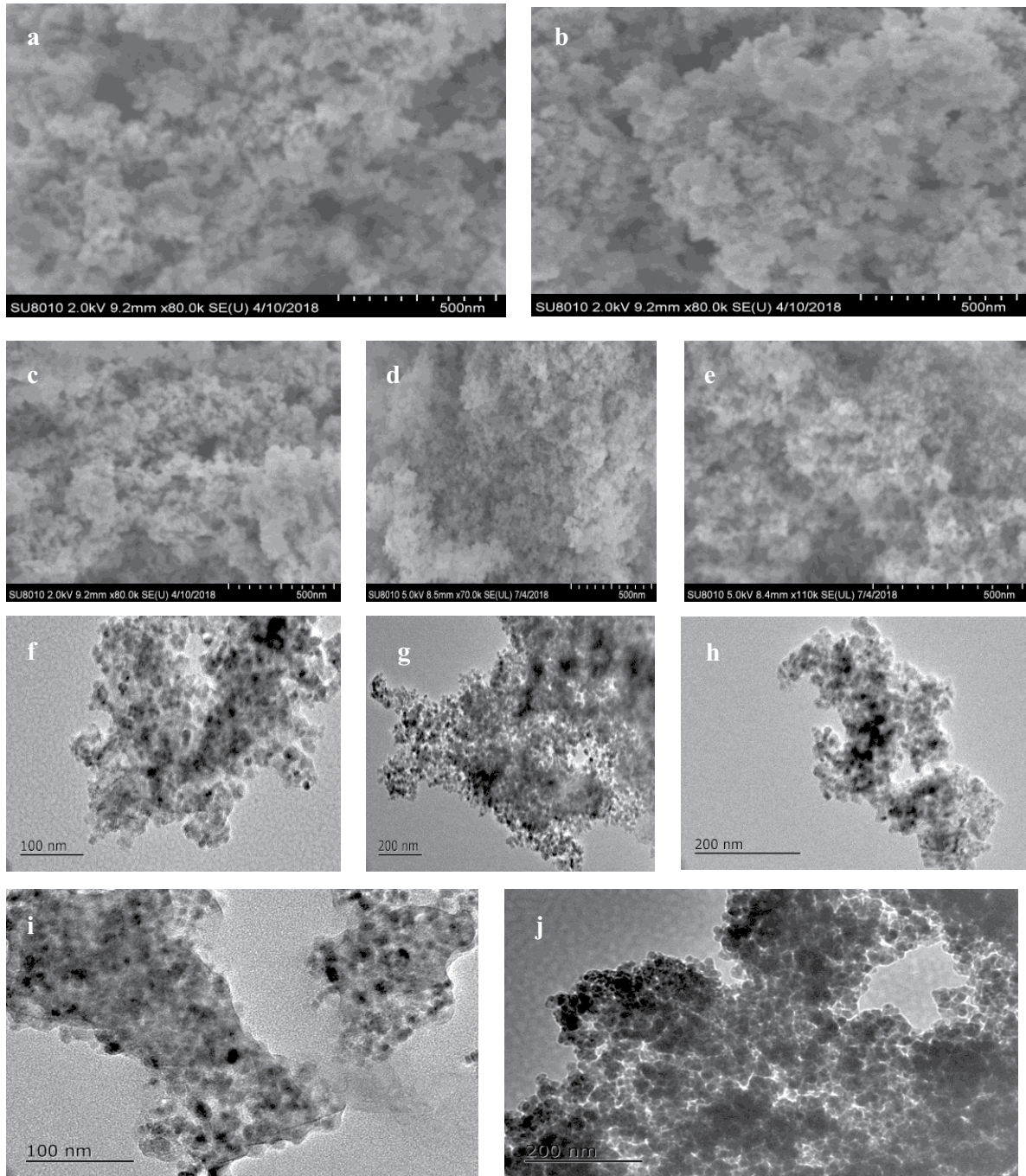


Fig. 3. Characterization of the superparamagnetic micro-sorbents through SEM (a–e) and TEM (f–j) (a) a, f, bare $\text{Fe}_3\text{O}_4@SiO_2$, (b) b, g, MgAl-NP, (c) c, h, MgFe-NP, (d) d, i, MgAlHf-NP, and (e) e, j, MgFeHf-NP.

the diameter ranged from 10 to 50 nm, with shell thickness roughly estimated to be less than 10 nm. Although coating with silica as a layer and hydrous metal oxides resulted in a coarse surface; the original structure of magnetite was on the whole maintained. The particle size of the composite material is small, and the particle size is between 20 and 60 nm. The rough surface of composite can increase its specific surface area and enhance its adsorption capacity.

Fig. 4 shows the XRD pattern of the composites. Specifically, strong peaks can be observed at 2θ values of 30.8° , 35.4° , 43.1° , 57.7° and 62.8° , indicating the spinel characteristic of magnetite (Fe_3O_4) that has been reported by many studies [20,21]. As is shown by XRD patterns, after coating with hydroxides and Hf, no new peaks emerged and the peaks above were not significantly affected. The curve peak type in the figure was not obvious and there were no disordered and new peaks, indicating the high purity of the nano-material. It also showed that the supported SiO_2 , hydroxides, and Hf had no clear crystal structure [22].

According to M-H curves (not shown), the bare Fe_3O_4 had the greatest saturated magnetization value of 79.44 emu/g, while the saturated magnetizations for MgAl-, MgFe-, MgAlHf-, MgFeHf-NPs were 45.90, 46.58, 41.63, 42.07 emu/g, separately. Mesoporous silica coating led to

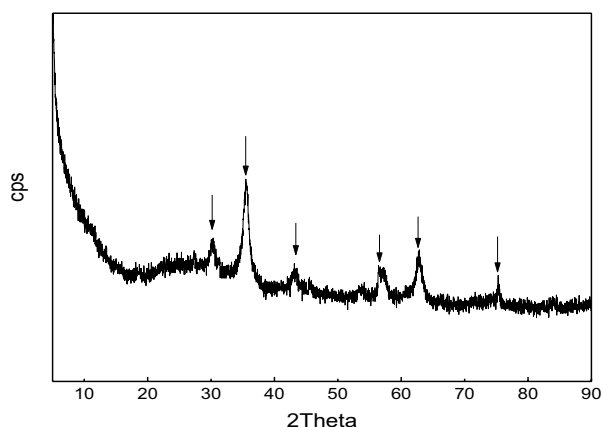


Fig. 4. XRD patterns of composite material. Arrows show the diffraction peaks arose from magnetite.

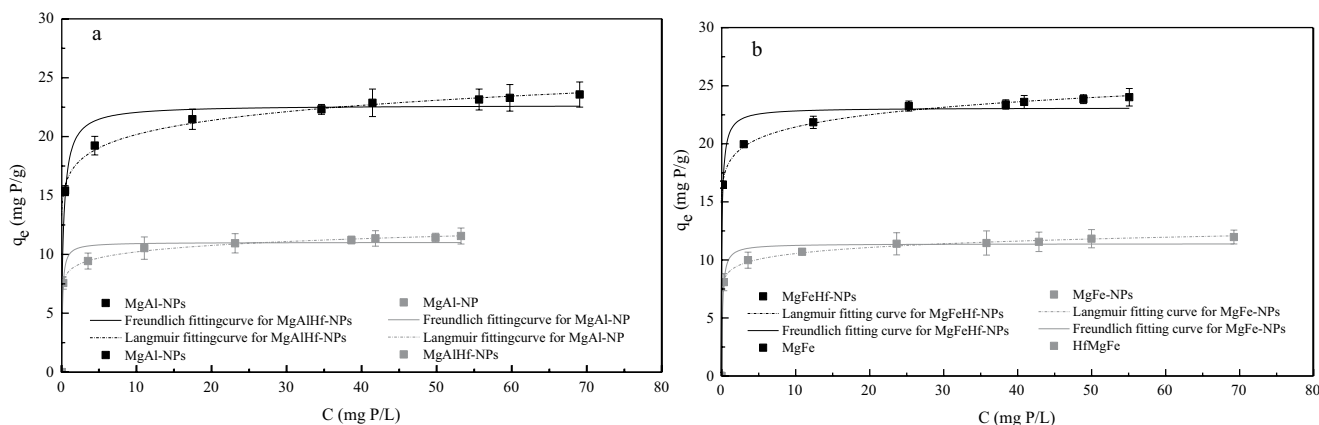


Fig. 5. Isotherms for phosphate adsorption on NPs: (a) MgAl-NPs and MgAlHf-NPs and (b) MgFe-NPs and MgFeHf-NPs.

the magnetization loss, and Hf loading resulted in a further loss. Nevertheless, saturation magnetization of 18–24 emu/g was reported to be sufficient to extract the particles from solutions with standard magnetic separation methods. And the Hf-coated superparamagnetic NPs seemed to process higher magnetization than the reported Zr- or La-coated ones, therefore allowing easier magnetic separation.

3.2. Adsorption isotherms

Once the superparamagnetic particles were added to the sewage, phosphate diffuses from the bulk solution to the surface of the adsorbent, and phosphate adsorption occurs. When superparamagnetic particles adsorb phosphate, phosphate reacts with intermediate layer ions directly, which enhances the selective adsorption of phosphate [23,24]. In this study, Fe_3O_4 @ SiO_2 showed little adsorption capacity for phosphate ions (data not shown), indicating oxide/hydroxide substances were the real center that adsorption occurs while magnetite embedded in a SiO_2 matrix acted as core and carriers. Fig. 5 presents the phosphate adsorption on the NPs plotted against different phosphate equilibrium concentrations, with fitting results and parameter values of Langmuir and Freundlich are obtained from Table 3. It can be inferred from the correlation coefficient in the table that the isotherm figures were more propitious to the Langmuir equation for all types of adsorbents, which assumes monolayer coverage of a heterogeneous adsorbent surface. The functionalization of hydrous hafnium oxide on the magnetite core-shell material caused the q_m value of 22.69 and 23.09 mg/g for MgAlHf-NP and MgFeHf-NP, compared with 11.02 and 11.39 mg/g for MgAl-NP and MgFe-NP. It shows that the Hf-modified complex adsorbent has a larger adsorption capacity and improves the adsorption selectivity to phosphate. Thus, Hf-loading changed the surface characteristic and enhanced the phosphate adherence onto the nano-sorbents.

3.3. Effect of coexisting anions and biomacromolecules on phosphate adsorption by superparamagnetic NPs

The source of domestic sewage is complex, and usually there are different anions in sewage. The nano-sorbent

Table 3

Langmuir and Freundlich equation parameters of phosphate adsorption onto (a) MgAl-NPs and MgAlHf-NPs and (b) MgFe-NPs and MgFeHf-NPs

Types of NPs	Langmuir			Freundlich		
	q_m	K_L	R^2	K_f	$1/n$	R^2
MgAl-NPs	11.0237	3.5466	0.9746	8.5999	0.0747	0.9922
MgFe-NPs	11.3932	7.8156	0.9799	18.2379	0.0699	0.9928
MgAlHf-NPs	22.6927	9.7295	0.9817	16.6420	0.1028	0.9899
MgFeHf-NPs	23.0940	8.1713	0.9803	8.9878	0.0696	0.9876

would inevitably encounter many complicated impurities in aquatic systems, which might compete with phosphate for adsorption sites on the surface of NPs. Taking digester liquor as an example, phosphate generally coexisted with short chain fatty acid, extracellular polymeric substances such as polysaccharide and protein [25]. The presence of Cl^- and SO_4^{2-} had insignificant effect on the adsorption of phosphate even if with higher concentration than phosphate [26]. To obtain pure targeted phosphate, the adsorption performance of superparamagnetic NPs should not be essentially affected by other impurities. Preceding research investigating interferential effect mainly concentrate on the coexisting anions, such as Cl^- , SO_4^{2-} , CO_3^{2-} , etc. Superparamagnetic nanocomposites will preferentially adsorb these anions competing with phosphate, resulting in the decrease of phosphate adsorption capacity of the composite. Nevertheless, anions from short-chain aliphatic acid as well the hydrophilic groups on biomacromolecules in digester liquor might also have competitive effect on phosphate recovery. Herein, the effects of these foreign materials, Cl^- , SO_4^{2-} , CH_3COO^- (10 mM), polysaccharide (sodium alginate, 100 mg/L, Yuanye Biological Technology Co. Ltd., Shanghai) and protein (bovine serum albumin, 100 mg/L, Yuanye Biological Technology Co. Ltd., Shanghai), on the phosphate adsorption were examined, with results manifested in Fig. 6.

The incipient concentration of phosphate was 5 mg P/L (16 mM), 88.2%, 88.4%, 97.2%, 93.8% of which can be captured by 0.5 g/L MgAl-, MgAlHf-, MgFeHf-, MgAlHf-NPs, respectively. For MgAl- and MgFe-NPs, anions of SO_4^{2-} , Cl^- , CH_3COO^- (10 mM), even at much higher concentrations than that of phosphate, had no or slight effect on the phosphate adsorption. Biomacromolecules of protein and polysaccharide (100 mg/L) seemed having competitive effect for adsorption sites. In contrast, Hf-coated nanoparticles exhibited high selectivity toward phosphate ions, in spite of high concentrations of coexisting anions and biomacromolecules. This clearly implied that the reaction mechanism of phosphate onto the nanoparticles were different from that of SO_4^{2-} and Cl^- ions. As previous literatures stated, phosphate can be strongly adsorbed because of the ligand exchange, while SO_4^{2-} , NO_3^- , Cl^- were adsorbed by electrostatic attraction [14,26]. The competing adsorptive behaviors of biomacromolecules onto the plain nanoparticles indicated the similar adsorption mechanism to that of phosphate. In contrast, Hf-coated nanoparticles showed high selectivity towards phosphate in presence of protein and polysaccharide, indicating that hydrous hafnium oxide strengthened

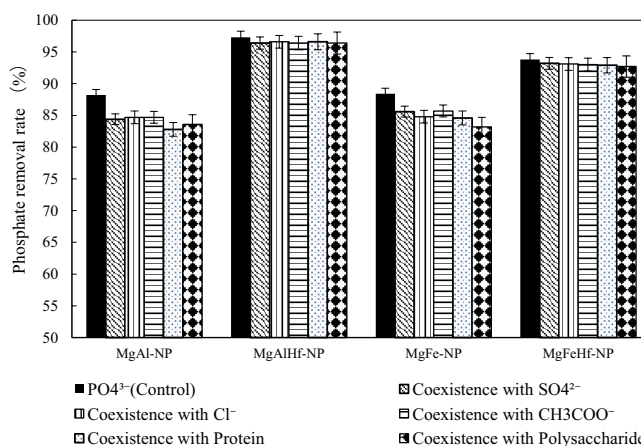


Fig. 6. Effect of coexisting substances on the phosphate removal performance of NPs.

the ligand exchange of phosphate with the hydroxyl groups on the surface. Therefore, phosphate capture from the wastewater with high strength of sludge extracellular polymeric substances, for example, anaerobic digestion liquor, can be successfully realized with Hf-NPs.

3.4. Phosphate uptake from DSL and DSW

For acidified DSL or DSW, large proportion of orthophosphate solved during acidification can be recovered with Hf-NPs (Fig. 7). As indicated by Fig. 8, about 90% of phosphate were captured with Hf-NPs either from DSL or DWL (Fig. 8). Or-P seemed decreased little after treating with nano-sorbents. For example, orthophosphate and or-P in raw DSW (Plant 1), with original value of 43.6 and 12.3 mg/L and were removed by about 90% and <1%, respectively, with 1 g/L Hf-NPs, rose to 176.1 and 14.5 mg/L at pH 4 (Fig. 7), and then treated with Hf-NPs, resulting in removal rates of 77.76% and <1%. Therefore, or-P seemed being excluded from the adsorption matrix due to the high selectivity of the nanoparticles. As a matter of fact, the most important factor greatly hindering the application of this material is the high cost on NPs consumption. According to our recent semi-continuous test with lab-scale phosphate recovery reactor dosing NPs, a total of 24.9 g of phosphorus could be produced from 1 m³ at the expense of dosing 12.6 g similar nano-sorbent, that is, 13.8 RMB/m³. Therefore, more efforts should be devoted to developing more excellent and cost-effective sorbents with large phosphate

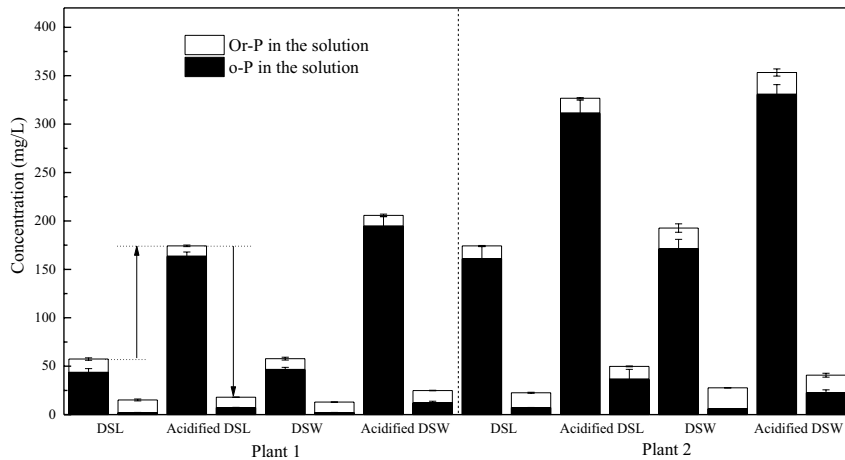


Fig. 7. Or-P and o-P concentrations in DSL and DSW before and after acidification treatment.

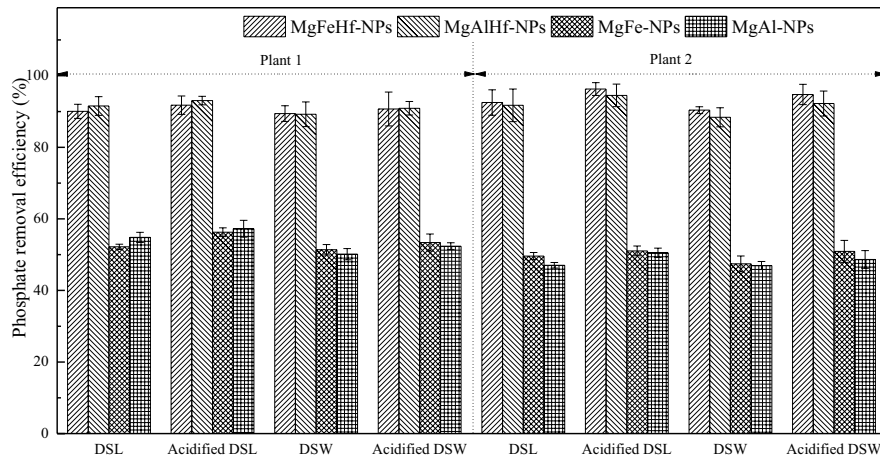


Fig. 8. Phosphate remove efficiency from DSL and DSW with NPs.

uptake capacity, high selectivity, high magnetization for fast separation and high reusability in multiple cycles.

It is worth noting that adsorption capacity for DSL and DSW was roughly the same with the analog value indicated by the Freundlich model while the ones for the acidified DSL and DSW were all above the analog value, especially for the larger equilibrium concentrations. This implied that acidification pretreatment for sludge would contribute to higher phosphate uptake by Hf-NPs from DSL and DSW probably due to not only the solution of orthophosphate from raw sludge but also the low pH preference of the NPs. Lundehoj et al. [27] reported the LDH (layered double hydroxides)-based materials' preference for acidic solution, and our research confirmed the similar adsorption behavior exhibited by hydroxides-based NPs.

Table 4 shows compositions of DSL and DSW before and after adsorption with La-nano-sorbents (La-NPs). It can be seen that Cl^- , Mg^{2+} and pH increased slightly while other items, such as NO_3^- , HCO_3^- , SO_4^{2-} and organic compositions were almost stable, suggesting the high selectivity of doped NPs towards phosphate in presence of other background ions. This clearly implied that the reaction mechanism of

phosphate onto the nanoparticles was different from that of SO_4^{2-} and Cl^- ions [14,26]. Biomacromolecules, for example, short chain fatty acid, extracellular polymeric substances such as polysaccharide and proteins, also showed no significant interferential effect on phosphate adsorption, although some of these biomacromolecules might form complicated intermolecular network or even be capable of being separated by NiAl-nanoparticles [28–30].

3.5. Role of Hf: mechanism analysis for adsorption

As for the superparamagnetic particle sorbents, the hydroxides-based NPs showed different structure as indicated by the TEM, SEM, XRD patterns [29]. But they contained hydroxyl groups on the surface or interlayer space, which can adsorb phosphate ions by mechanisms of electrostatic attraction, ligand complexation and/or surface precipitation [31]. It has been widely in presence of other anions such as Cl^- , NO_3^- and SO_4^{2-} that were adsorbed by electrostatic attraction [32,33]. The high selectivity showed in section 3.3 suggested that ligand reaction might have also took the main responsibility for hydroxides-based NPs.

Table 4
Compositions of DSW and DSL before and after adsorption with MgAlHf-NPs

Item (mg/L)	Raw DSL	After Adsorption	Raw DSW	After Adsorption	Acidified DSL	After Adsorption	Acidified DSW	After adsorption
Plant 1								
HCO ₃ ⁻	75.6	79.2	100.6	102.8	ND ^a	ND	ND	ND
Cl ⁻	81.0	90.1	217.4	228.9	127.9	125.3	260.4	263.3
SO ₄ ²⁻	29.4	28.2	35.8	34.0	27.3	26.9	34.1	33.4
NO ₃ ⁻	ND	ND	12.57	11.2	ND	ND	10.5	9.8
Fe ³⁺	6.6	6.9	2.9	3.0	8.7	9.4	12.0	10.1
Ca ²⁺	5.4	6.0	6.2	6.6	29.5	28.6	44.9	48.5
Mg ²⁺	0.1	0.1	1.0	1.4	8.1	12.9	7.6	16.7
EPS Protein	25.6	25.1	44.2	44.0	132.4	129.8	142.6	138.2
Polysacc-haride	23.8	22.9	43.8	42.5	120.5	120.3	128.3	127.2
pH	6.8	7.6	6.7	7.6	3	3.6	3	3.6
Plant 2								
HCO ₃ ⁻	39.4	42.5	102.0	103.1	ND	ND	ND	ND
Cl ⁻	173.9	177.0	120.3	123.4	231.6	235.2	163.5	164.9
SO ₄ ²⁻	10.7	9.4	12.4	11.8	9.7	7.3	8.7	5.6
NO ₃ ⁻	ND	ND	ND	ND	ND	ND	ND	ND
Fe ³⁺	ND	ND	ND	ND	ND	ND	ND	ND
Ca ²⁺	1.3	1.2	3.5	3.7	51.8	51.7	27.3	29.1
Mg ²⁺	2.2	2.7	3.0	3.0	16.5	16.1	25.3	25.7
EPS Protein	132.7	131.6	159.0	157.7	328.2	325.5	319.4	318.2
Polysaccharide	102.4	100.3	119.1	115.6	372.0	368.1	396.1	397.0
pH	6.6	6.9	6.6	7.0	3	3.2	3	3.3

^aNot detected.

Moreover, Hf's role in strengthening phosphate adsorption can be explained by the theory of hard and soft acids bases. Ligand complexation was believed to be the dominant mechanism for phosphate adsorption since NPs showed high selectivity towards phosphate, which can be considered as the formation of acid-base complexes – A:B (A+:B---A:B), where A is an electron acceptor or electrophile, regarded as the acid and B is the electron donor, regarded as the base. Acid and bases can be labelled as hard or soft according to their charge, size, polarization or other characteristics [34]. The combination of hard-hard or soft-soft could establish extra stabilization. Generally, cations of Mg²⁺, Fe³⁺, Al³⁺ were harder acid than the transitional metal ion Hf⁴⁺, and meanwhile phosphate ions were relatively softer base than Cl⁻, SO₄²⁻. Therefore Hf⁴⁺ and phosphate in this study seemed a pair that matched up the bonding preferences, forming stronger ligand complexation [35].

3.6. Desorption, regeneration and reusability

The repetitions of phosphate adsorption/desorption for different types of NPs are shown in the heatmap in Fig. 9. For the first cycle, the phosphate recovery rates were 92.7%, 96.0%, 92.0% and 96.5% for MgAl-, MgAlHf-, MgFe-, MgAlHf-NPs, respectively. The desorption amounts were very close to the uptake amount in adsorption test for all the nano-sorbents. Thus, it can be inferred that a complete

desorption (100%) was almost achieved on each material via 3 M NaOH at 30°C. The adsorption capacities of the retrieved nanomaterials decreased with cycles of regenerations, leading to the decreasing recovery rates correspondingly. After five cycles of adsorption and desorption, Hf-modified nano-sorbent still can achieve recovery rate of 80%, the mass loss of the material during the cycle resulted in about 20% loss of adsorption capacity, while plain nano-sorbent would suffer from nearly 50% of loss due to limited adsorption capacity. It was probably due to the stronger binding between Hf and phosphate during the adsorption stage, and complete release and recovery resulted from sufficient OH concentration and clear pH shift during the desorption/regeneration. This phenomenon was consistent with previous literatures that caustic alkalinity was one of the important factors that influenced phosphate release and desorption rate [36]. Sufficient dose of nano-sorbent, high level of pH as well as high temperature can ensure high efficiency of P-uptake and recovery [37]. Besides, the poorer performance after cycles of reaction was caused by both NPs loss/leakage and increasing "inert adsorption site" which might have resulted from incomplete desorption or regeneration.

4. Conclusions

This work proposes that a novel magnetically separable and reusable Hf-hydroxide-based nano-sorbent to

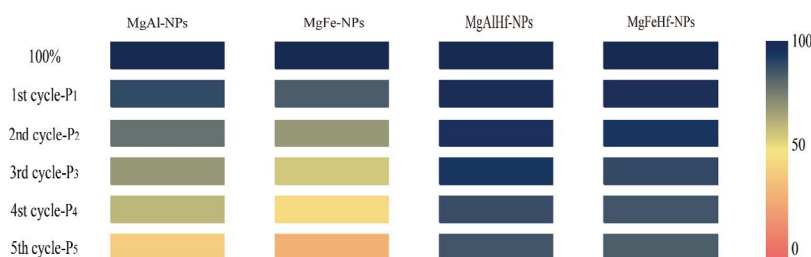


Fig. 9. Recovery percentage (Pi value) of phosphate loaded on the nano-sorbents during 5 cycles of adsorption–desorption.

efficiently capture and recover phosphate from sewage and superparamagnetic nanocomposites with better phosphate adsorption effect are prepared by the improved microwave hydrothermal method. The NPs were successfully prepared, exhibiting crystal structures as well as sufficient saturated magnetization value for fast separation in magnetic field. The isotherm data were better fitted to the Freundlich model than Langmuir model for all types of NPs. The isotherm data indicated that Hf-loading changed the surface characteristic and improved the phosphate adherence onto the NPs. Besides, the competing anions and biomacromolecules had little effect on the phosphate adsorption. These NPs showed good performance of recovering phosphate from in DSL and DSW. The Hf-modified NPs' high adsorption capacity and selectivity toward phosphate ions should be attributed to the fact that hard acid Hf^{4+} and hard base phosphate matched up the bonding preferences and therefore formed stronger ligand complexation. The MgAlHf/MgFeHf-NPs were competitive in terms of adsorption capacity, selectivity and reusability. Based on the concept of “energy self-sufficiency and resource recovery” in sewage treatment, this study increased the reuse of phosphorus resources and realized the optimal allocation of resources.

Acknowledgements

The authors would like to thank National Natural Science Foundation of China Projects (grant number 51708338, 2017), (grant number 51878394, 2018) and (grant number 51808019, 2018). This work was also supported in part by funded by the Research Fund Program of Guangdong Provincial Key Laboratory of Environmental Pollution Control and Remediation Technology, Doctoral Research Fund of Shandong Jianzhu University (grant number XNBS1702, 2018) and Youth Innovation Technology Project of Higher School in Shandong Province (2019KJD003).

References

- [1] P. Wilfert, A.I. Dugulan, K. Goubitz, L. Korving, G.J. Witkamp, M.C.M. Van Loosdrecht, Vivianite as the main phosphate mineral in digested sewage sludge and its role for phosphate recovery, *Water Res.*, 144 (2018) 312–321.
- [2] P. Battistoni, A. De Angelis, P. Pavan, M.C.F. Prisciandaro, Phosphorus removal from a real anaerobic supernatant by struvite crystallization, *Water Res.*, 35 (2001) 2167–2178.
- [3] K. Shimamura, T. Kurosawa, Phosphorus recovery using a crystallization process for sewage treatment plant, *Water Pract. Technol.*, 6 (2011), doi: 10.2166/wpt.2011.064.
- [4] D. Kim, H.D. Ryu, M.S. Kim, J. Kim, S.I. Lee, Enhancing struvite precipitation potential for ammonia nitrogen removal in municipal landfill leachate, *J. Hazard. Mater.*, 146 (2007) 81–85.
- [5] L. Pastor, D. Mangin, R. Barat, A. Seco, A pilot-scale study of struvite precipitation in a stirred tank reactor: conditions influencing the process, *Bioresour. Technol.*, 99 (2008) 6285–6291.
- [6] K.P. Fattah, Y. Zhang, D.S. Mavinic, F.A. Koch, Use of carbon dioxide stripping for struvite crystallization to save caustic dosage: performance at pilotscale operation, *J. Environ. Eng. Sci.*, 8 (2013) 575–579.
- [7] C.K. Chauhan, M.J. Joshi, In vitro crystallization, characterization and growth-inhibition study of urinary type struvite crystals, *J. Cryst. Growth*, 362 (2013) 330–337.
- [8] R.L. Knight, B. Gu, R.A. Clarke, J.M. Newman, Long-term phosphorus removal in Florida aquatic systems dominated by submerged aquatic vegetation, *Ecol. Eng.*, 20 (2003) 45–63.
- [9] R.J. Chiou, Y.R. Yang, An evaluation of the phosphorus storage capacity of an anaerobic/aerobic sequential batch biofilm reactor, *Bioresour. Technol.*, 99 (2008) 4408–4413.
- [10] F. Rogalla, T.L. Johnson, J. McQuarrie, Fixed film phosphorus removal—flexible enough, *Water Sci. Technol.*, 53 (2006) 75–81.
- [11] E. Paul, M.L. Laval, M. Sperandio, Excess sludge production and costs due to phosphorus removal, *Environ. Technol.*, 22 (2001) 1363–1371.
- [12] A. Drenkova-Tuhtan, M. Schneider, M. Franzreb, C. Meyer, C. Gellermann, G. Sextl, K. Mandel, H. Steinmetz, Pilot-scale removal and recovery of dissolved phosphate from secondary wastewater effluents with reusable ZnFeZr adsorbent@ $\text{Fe}_3\text{O}_4/\text{SiO}_2$ particles with magnetic harvesting, *Water Res.*, 109 (2017) 77–87.
- [13] K. Mandel, A. Drenkova-Tuhtan, F. Hutter, C. Gellermann, H. Steinmetz, G. Sextl, Layered double hydroxide ion exchangers on superparamagnetic microparticles for recovery of phosphate from waste water, *J. Mater. Chem., A1* (2013) 1840–1848.
- [14] M. Chen, C. Huo, Y. Li, J. Wang, Selective adsorption and efficient removal of phosphate from aqueous medium with graphene–lanthanum composite, *ACS Sustainable Chem. Eng.*, 4 (2016) 1296–1302.
- [15] L. Lai, Q. Xie, L. Chi, W. Gu, D. Wu, Adsorption of phosphate from water by easily separable $\text{Fe}_3\text{O}_4/\text{SiO}_2$ core/shell magnetic nanoparticles functionalized with hydrous lanthanum oxide, *J. Colloid Interface Sci.*, 465 (2016) 76–82.
- [16] C. Zhang, Y. Li, F. Wang, Z. Yu, J. Wei, Z. Yang, C. Ma, Z. Li, Z. Xu, G. Zeng, Performance of magnetic zirconium-iron oxide nanoparticle in the removal of phosphate from aqueous solution, *Appl. Surf. Sci.*, 396 (2017) 1783–1792.
- [17] Chunming Su, R.W. Puls, Arsenate and arsenite removal by zerovalent iron: effects of phosphate, silicate, carbonate, borate, sulfate, chromate, molybdate, and nitrate, relative to chloride, *Environ. Sci. Technol.*, 35 (2001) 4562–4568.
- [18] B. Frølund, R. Palmgren, K. Keiding, P.H. Nielsen, Extraction of extracellular polymers from activated sludge using a cation exchange resin, *Water Res.*, 30 (1996) 1749–1758.
- [19] K. Raunkjær, T. Hvitved-Jacobsen, P.H. Nielsen, Measurement of pools of protein, carbohydrate and lipid in domestic wastewater, *Water Res.*, 28 (1994) 251–262.

- [20] S. Rajput, C.U. Pittman, D. Mohan, Magnetic magnetite (Fe_3O_4) nanoparticle synthesis and applications for lead (Pb^{2+}) and chromium (Cr^{6+}) removal from water, *J. Colloid Interface Sci.*, 468 (2016) 334–346.
- [21] L.B. Tahar, M.H. Oueslati, M.J.A. Abualreish, Synthesis of magnetite derivatives nanoparticles and their application for the removal of chromium(VI) from aqueous solutions, *J. Colloid Interface Sci.*, 512 (2018) 115–126.
- [22] C.A. Gorski, M.M. Scherer, Determination of nanoparticulate magnetite stoichiometry by Mössbauer spectroscopy, acidic dissolution, and powder X-ray diffraction: a critical review, *Am. Miner.*, 95 (2010) 1017–1026.
- [23] R. Chitrakar, S. Tezuka, A. Sonoda, K. Sakane, K. Ooi, T. Hirotsu, Synthesis and phosphate uptake behavior of Zr^{4+} incorporated MgAl-layered double hydroxides, *J. Colloid Interface Sci.*, 313 (2007) 53–63.
- [24] L. Fang, R. Liu, J. Li, C. Xu, L.Z. Huang, D. Wang, Magnetite/Lanthanum hydroxide for phosphate sequestration and recovery from lake and the attenuation effects of sediment particles, *Water Res.*, 130 (2018) 243–254.
- [25] P. Van Rensburg, E.V. Musvoto, M.C. Wentzel, G.A. Ekama, Modelling multiple mineral precipitation in anaerobic digester liquor, *Water Res.*, 37 (2003) 3087–3097.
- [26] Y. Su, H. Cui, Q. Li, S. Gao, J.K. Shang, Strong adsorption of phosphate by amorphous zirconium oxide nanoparticles, *Water Res.*, 47 (2013) 5018–5026.
- [27] L. Lundehoj, H.C. Jensen, L. Wybrandt, U.G. Nielsen, M.L. Christensen, C.A. Quist-Jensen, Layered double hydroxides for phosphorus recovery from acidified and non-acidified dewatered sludge, *Water Res.*, 153 (2019) 208–216.
- [28] R. Wang, D. Liang, X. Liu, W. Fan, S. Meng, W. Cai, Effect of magnesium ion on polysaccharide fouling, *Chem. Eng. J.*, 379 (2020) 122351.
- [29] M. Shao, F. Ning, J. Zhao, M. Wei, D.G. Evans, X. Duan, Preparation of $\text{Fe}_3\text{O}_4@\text{SiO}_2$ -layered double hydroxide core-shell microspheres for magnetic separation of proteins, *J. Am. Chem. Soc.*, 134 (2012) 1071–1077.
- [30] S. Meng, W. Fan, X. Li, Y. Liu, D. Liang, X. Liu, Intermolecular interactions of polysaccharides in membrane fouling during microfiltration, *Water Res.*, 143 (2018) 38–46.
- [31] A.V. Radha, P.V. Kamath, C. Shivakumara, Mechanism of the anion exchange reactions of the layered double hydroxides (LDHs) of Ca and Mg with Al, *Solid State Sci.*, 7 (2006) 1180–1187.
- [32] H. He, H. Kang, S. Ma, Y. Bai, X. Yang, High adsorption selectivity of ZnAl layered double hydroxides and the calcined materials toward phosphate, *J. Colloid Interface Sci.*, 343 (2010) 225–231.
- [33] Y. Qiangqiang, Y. Zheng, Y. Wang, L. Shen, H. Wang, Y. Zheng, N. Hea, Q. Li, Highly selective adsorption of phosphate by pyromellitic acid intercalated ZnAl-LDHs: assembling hydrogen bond acceptor sites, *Chem. Eng. J.*, 260 (2015) 809–817.
- [34] G. Makov, Chemical Hardness in Density Functional Theory, *J. Phys. Chem.*, 99 (1995) 9337–9339.
- [35] R.G. Pearson, Recent advances in the concept of hard and soft acids and bases, *J. Chem. Educ.*, 64 (1987) 561–567.
- [36] T. Zhan, Y. Zhang, Q. Yang, H. Deng, J. Xu, W. Hou, Ultrathin layered double hydroxide nanosheets prepared from a water-in-ionic liquid surfactant-free microemulsion for phosphate removal from aquatic systems, *Chem. Eng. J.*, 302 (2016) 459–465.
- [37] M. Zubair, M. Daud, G. McKay, F. Shehzad, M.A. Al-Harathi, Recent progress in layered double hydroxides (LDH)-containing hybrids as adsorbents for water remediation, *Appl. Clay Sci.*, 143 (2017) 279–292.